Understanding the role of buried interface charges in a metal-oxide-semiconductor stack of Ti/Al2O3/Si using hard x-ray photoelectron spectroscopy

J. R. Church, C. Weiland, and R. L. Opila

Citation: Applied Physics Letters **106**, 171601 (2015); doi: 10.1063/1.4919448
View online: http://dx.doi.org/10.1063/1.4919448
View Table of Contents: http://scitation.aip.org/content/aip/journal/apl/106/17?ver=pdfcov
Published by the AIP Publishing

Understanding the role of buried interface charges in a metal-oxide-semiconductor stack of Ti/Al_2O_3/Si using hard x-ray photoelectron spectroscopy

J. R. Church,[1] C. Weiland,[2] and R. L. Opila[1]
[1]*University of Delaware, Newark, Delaware 19711, USA*
[2]*Synchrotron Research, Inc., Upton, New York 11973, USA*

(Received 12 December 2014; accepted 19 April 2015; published online 28 April 2015)

Hard X-ray photoelectron spectroscopy (HAXPES) analyses were carried out on metal-oxide-semiconductor (MOS) samples consisting of Si, thick and thin Al_2O_3, and a Ti metal cap. Using Si 1*s* and C 1*s* core levels for an energy reference, the Al 1*s* and Si 1*s* spectra were analyzed to reveal information about the location and roles of charges throughout the MOS layers. With different oxide thicknesses (2 nm and 23 nm), the depth sensitivity of HAXPES is exploited to probe different regions in the MOS structure. Post Ti deposition results indicated unexpected band alignment values between the thin and thick films, which are explained by the behavior of mobile charge within the Al_2O_3 layer. © *2015 AIP Publishing LLC*. [http://dx.doi.org/10.1063/1.4919448]

Ideally, deposited thin films would be studied in their un-affected, device ready state. Unfortunately, this approach makes chemical analyses of buried layers prohibitively difficult. There have, however, been advancements in synchrotron based photoemission techniques,[1] and in conjunction with the continued scaling of devices, interfacial regions of multilayered films are within probing distances. Given the high brilliance and energy ranges of hard X-ray photoelectron spectroscopy (HAXPES) chemical state as well as electronic information can be obtained non-invasively.[2–4] While numerous non-invasive elemental state analysis techniques like Raman spectroscopy, Auger electron spectroscopy (AES), or even standard X-ray photoemission spectroscopy (XPS) are available it may be difficult to quantify band alignments (Raman and AES), or will be prohibitively surface sensitive without further sample modification (AES and XPS).[5,6]

Exploiting the robust capabilities of HAXPES for elemental analyses and large probing distances allowed us to investigate the effects of oxide thickness on the band alignments within a metal-oxide-semiconductor (MOS) multilayer film. This technique is especially beneficial for modern electrical devices and chemical processes due to decreasing layer thicknesses and increasing importance of interfaces and energy band alignments. Our work demonstrates a powerful tool to elucidate the role that interlayer thickness plays in overall band alignments. With this in mind, HAXPES could foster significant advancements in work function (WF) engineering as industry attempts to optimize each layer's performance by selectively introducing novel material compositions; a non-exhaustive search in relevant work function engineering literature can be found elsewhere.[7–9]

Al_2O_3 was chosen for its wide band gap[10] and usage in solar cells and transparent thin film oxides.[11–13] Ti was chosen as a low WF metal with WF of $q\Phi_{m,vac} = 4.33$ eV.[14]

Al_2O_3 films were deposited on 100 mm p-type (10–20 Ω cm) Si(100) substrates. Al_2O_3 was deposited by atomic layer deposition (ALD) using trimethyl aluminum (TMA) and H_2O at 300 °C in a Picosun showerhead ALD system. Deposited Al_2O_3 thin films were 2 nm and 23 nm thick as determined by spectroscopic ellipsometry (not shown). Prior to Ti deposition, all samples were subjected to a thermal treatment of annealing (400 °C, 20 min) and firing (760 °C, 3 s). The firing step was similar to the one used for photovoltaics described elsewhere.[15] Ti deposition was carried out by evaporation using Cerac Ti pellets (99.8%) and a Thermionics VE-100 Vacuum Evaporator; deposition was carried out for 74 s at a rate of 0.07 nm/s as monitored by a quartz crystal microbalance (QCM) at a pressure of 3×10^{-6} Torr for a thickness of 5.2 nm. The uncapped 2 nm and 23 nm thermally treated samples will be referred to as 2-Al and 23-Al, respectively, and Ti capped films will be referred to as 2-Ti and 23-Ti with numbers indicating the appropriate Al_2O_3 thickness.

HAXPES experiments were carried out in ultra-high vacuum with end station pressure maintained below 2×10^{-8} Torr at National Institute of Standards and Technology (NIST) beam line ×24A at the National Synchrotron Light Source at Brookhaven National Laboratory. Wavelength selection was carried out by a double Si(111) crystal monochromator; feedback-stabilization was also used to compensate for thermal effects on the crystals. The photon energy range available was 2.1–5 keV. Final focusing was carried out by nickel-coated quartz toroidal mirror. Nominal beam energy adjustment was referenced using a clean silver foil, and the Ag $3d_{5/2}$ peak binding energy (BE) 368.3 eV (Ref. 16) which was detected by a Scienta R4000 hemispherical electron energy analyzer located at a take-off angle of 85° with a pass energy of 200 eV. We used a nominal photon energy of 4500 eV to excite core level electrons present in the Ti cap layer, Al_2O_3, and Si substrate. Strong signals from Al 1*s* and Si 1*s* core levels were present at this energy because of a large photoionization cross-section and were chosen over Al 2*p* and Si 2*p* levels for this reason. Like traditional XPS, we deduced peak BE shifts and peak intensities to infer chemical states and

energy band lineups. Approximate error associated with this measurement is +/− 50 meV.[17]

Differential charge correction is an important step in the analysis of XPS data, and for HAXPES data where photon energy may not be exactly known this step is especially crucial. In standard XPS, most X-rays are generated from either an Al or Mg filament which emits at known wavelengths 1486.6 eV and 1253.6 eV, respectively. Often charge correction and photon energy are determined using elemental peaks from a clean metal surface. Unfortunately, the challenge with this technique is that the photon energy may drift over time due to changing thermal loads on the monochromator, potentially skewing the energy referenced at an earlier time.

We use a modified adventitious carbon peak energy referencing method,[18] which can be used for future HAXPES studies. With a conductive channel to the sample surface to ground, elemental peaks from adventitious carbon and the silicon substrate were collected. Both of these reference spectra play a central role in our analysis. First, let us consider peak referencing to the adventitious carbon peak. Adventitious carbon is a layer of material that is seen to deposit on many samples when exposed to the atmosphere; as a result, the C 1*s* BE peak associated with this layer has been used with some success in the past. Of particular concern with this method is sample surfaces with high polarity, high density materials as in Al_2O_3.[19] Additionally, the adventitious carbon should be electrically isolated from the sample which may not be the case for a metalized surface.[18] To systematically correlate energy scales in each of our samples in this work, we used the adventitious carbon C 1*s* peak to complement the Si 1*s* peak energy as the primary reference. A strong signal from the Si bulk was available for both the thin samples 2-Al and 2-Ti with our HAXPES probe; which previous work on similarly doped substrates assigned a value of 1839.5 eV.[2,17] Shifting all peaks present in 2-Al and 2-Ti relative to their Si 1*s* peak, we now record the C 1*s* BE peaks as BE-Al and BE-Ti, respectively, and notice that indeed BE-Al and BE-Ti differ by a value of 0.45 eV.[20] For the thicker samples 23-Al and 23-Ti, the Si 1*s* peak intensity drops significantly and possesses an unacceptable signal-to-noise ratio, we then utilize the carbon C 1*s* peak collected from the thinner samples as a reference. Our complimentary peak referencing method is outlined below:

- Set the Si 1s BE to 1839.5 eV for samples 2-Al and 2-Ti. Shift all XPS spectra from 2-Al and 2-Ti relative to the Si 1*s* shifts; record the C 1*s* BE as BE-Al and BE-Ti, respectively. BE-Al and BE-Ti were found to be 286.15 eV and 285.7 eV, respectively.[20]
- Shift all spectra collected from sample 23-Al relative to the C 1*s* shift from BE-Al
- Shift all spectra collected from sample 23-Ti relative to the C 1*s* shift from BE-Ti

Fig. 1 shows a representation of the deposited films (Fig. 1(a)) and the Al 1*s* core level spectra (Fig. 1(b)). The interfacial regions present after deposition are denoted as IL-1 and IL-2 for the oxide and Ti metal deposition, respectively. Both 2-Al and 23-Al show no BE shift within the error but BE shifts of −0.17 eV and 0.33 eV were seen post metallization for 2-Ti and 23-Ti, respectively. Though 2-Al and 23-Al possessed the same BE, closer inspection of 2-Al reveals significant peak broadening compared to 23-Al (Table I). First, it is important to point out the IMFPs at the photon energy used are around 4–5 nm.[21] And, because of inelastic scattering, the thinner oxide samples were probing more Al 1*s* electrons near the Si interfacial layer IL-1 than in the thicker film. Previous work eliminates the possibility of peak broadening by sub-stoichiometric aluminum oxides or the presence of phase changes for similar temperatures and deposition methods.[22] Therefore, the conclusion made is that the broader peak width is indicative of an electric field on the Al_2O_3 side of IL-1.

The phenomenon initiating peak broadening of Al 1*s* peaks can be better understood by considering the electrical environment on the Si side of IL-1. Katamreddy *et al.* reported that there was growth of a thin interfacial SiO_x layer after heat treatments similar to this study.[22] The thin SiO_x contained fixed positive charges, most likely because of oxygen vacancies.[23–25] The presence of these positive charges attracts negative charges from both the Al_2O_3 and the Si substrate to IL-1, inducing dipoles on both sides. Confirmation of interfacial SiO_x growth is seen in Fig. 2, which shows the Si 1*s* spectra referenced to BE-Al for 23-Al before and after heat treatment. The silica peak (∼1843.5 eV) for the thermally treated sample shows significant intensity increase relative to the elemental peak, proof of a thicker interfacial SiO_x layer. Additionally, the elemental Si 1*s* peak shifted −0.21 eV (referenced to BE-Al) after thermal treatments which can be explained by the presence of increased electron density at the surface of the substrate.

Metal deposition in our MOS structure created a second interface, seen in Fig. 1 as IL-2. After metallization, there were three locations for charge accumulation: IL-1, IL-2, and the surface of the Si substrate. As discussed earlier, the presence of positive charge near IL-1 attracts electrons. For IL-2, the proposed mechanism of charge transfer is known as the "second nearest neighbor effect." Electron density in the

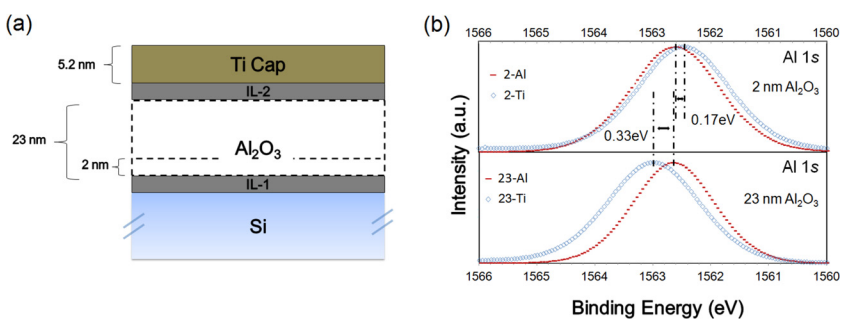

FIG. 1. (a) Visual representation of the deposited films. Interfacial region IL-1 is present post-Al_2O_3 deposition and IL-2 is present post-Ti deposition. Dashed lines represent the two different thicknesses of Al_2O_3. Not to scale. (b) Normalized Al 1*s* XPS spectra for samples 2-Al and 2-Ti (top) and samples 23-Al and 23-Ti (bottom). $\lambda_{Al1s} = 5.58$ nm at photon energy $h\nu = 4500$ eV.

TABLE I. BE and full width at half maximum (FWHM) of Al 1*s* core levels obtained for all samples.

	Al 1*s*	
Sample	BE (eV)	FWHM (eV)
2-Al	1562.64	1.85
2-Ti	1562.47	1.89
23-Al	1562.66	1.67
23-Ti	1562.99	1.82

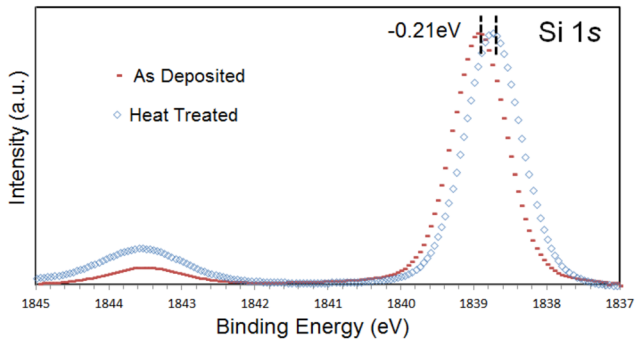

FIG. 2. Si 1*s* spectra for 23 nm Al_2O_3 before and after thermal treatments (annealing and firing). Peak intensities normalized to the elemental Si peaks to demonstrate increase in intensity of the satellite peak at 1843.5 eV, identified as the signal from SiO_x interfacial layer IL-1. $\lambda_{Si1s} = 4.83$ nm at photon energy $h\nu = 4500$ eV.

oxide layer will increase because of the more electron donating nature of Ti relative to aluminum or oxygen.[26] There is also evidence of similar charge transfer in other metal-oxide systems.[27]

The location of mobile charges as well as the proposed band diagram can be seen in Fig. 3. Presence of induced charges in the Al_2O_3 does not necessarily preclude the existence of fixed charges, but is beyond the scope of the present study. To quantify the role of charges in this MOS system, we need to consider the expected voltage drop across the oxide known as the flat-band voltage. For the ideal case, which ignores charge in the insulating oxide layer, the flat-band voltage for a Ti metal and a p-type Si substrate is the difference between the Ti WF, 4.33 eV, and the Si WF, $q\Phi_s = 4.87$ eV.[17] Therefore, the ideal case would give a flat band voltage drop equal to $q\Phi_{ms} = 0.54$ eV.

It is possible to track the potential drop in the oxide by monitoring the photoemission peak shifts from that layer; in this case, it is the Al 1*s* core level. The potential drop in our film stack demonstrated only at 0.33 eV BE shift in the Al 1*s* peak between samples 23-Al and 23-Ti (Fig. 1(b)), which is 0.21 eV smaller than the expected $q\Phi_{ms}$. Then, the suggestion is to conclude the presence of negative charge in the Al_2O_3 layer.

Effects of negative charge in the oxide can be understood by decreasing the separation between IL-2 and IL-1, which will enhance electrical influence the two interfaces

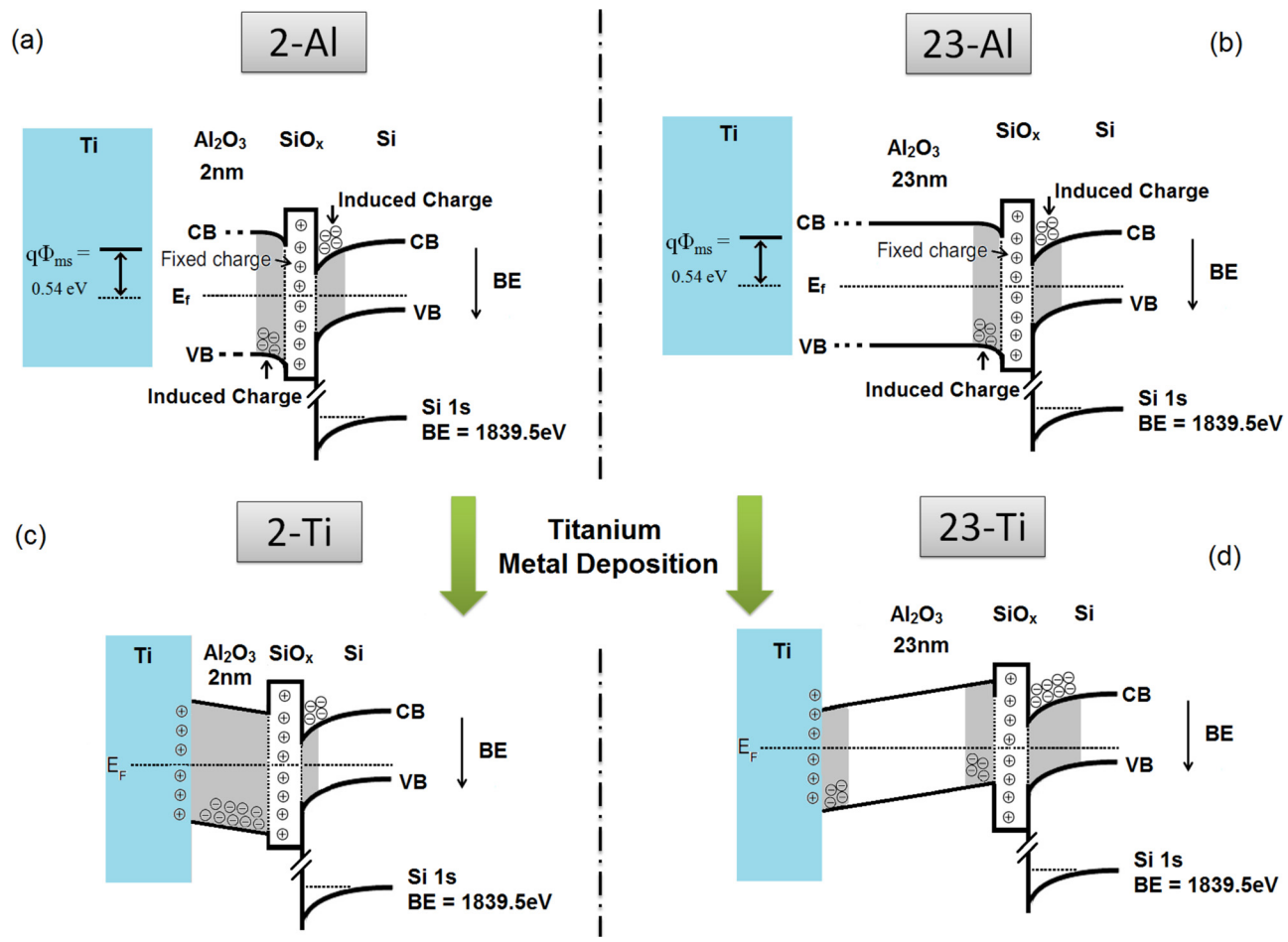

FIG. 3. Energy band diagram for the uncapped thin 2 nm Al_2O_3 film (a) and thick 23 nm Al_2O_3 (b) and Ti capped thin (c) and thick (d) films. Gray areas denote location of mobile charge throughout the film stack.

exert on each other. This situation is demonstrated in the Al 1*s* spectra of 23-Ti and 2-Ti, Fig. 1(b). The metallic cap layer acts as a source of electrons so that there would be an increased electron density in the Al_2O_3 if the attraction is strong enough. The presence of increased electron density causes a BE decrease in 2-Al's Al 1*s* spectrum after metallization. This behavior is not observed in 23-Al because the film's Al 1*s* spectrum is dominated by the charge neutral bulk region. Combining the thin and thick film BE difference gives 0.52 eV (Table I), which is in good agreement with the expected value of 0.54 eV.

Given the decreasing thicknesses in material stacks used in modern devices, the electrical and chemical processes taking place on smaller scales will play larger roles. In consideration of the present study, one could imagine work function engineering by only varying the thickness of the oxide. No other material or process changes would be needed. Already interfacial charges have been used for their beneficial screening and passivating properties,[25,28] HAXPES analysis would enhance the characterization of similar material systems.

In summary, we have used elemental HAXPES BE shifts to characterize the energy band alignment in a MOS stack of $Ti/Al_2O_3/Si$. The movement of the Al 1*s* core level before and after metal deposition indicated dissimilar potential differences across the thick oxide and the thin oxide interlayers. The dissimilarities are consistent with negative charges in the Al_2O_3 layer accumulating near positive charges in the interfacial SiO_x. This demonstrates the benefit of characterization techniques like HAXPES to probe buried material layers for electrical environments and chemical and elemental state analyses; thereby, supporting the development of band engineering concepts.

The authors wish to thank the U.S. Department of Energy, Office of Science, and Office of Basic Energy Sciences for the use of the National Synchrotron Light Source, Brookhaven National Laboratory which was supported under Contract No. DE-AC02-98CH-10886. The authors would also like to thank Air Liquide for the Al_2O_3 depositions.

[1]R. Claessen, M. Sing, M. Paul, G. Berner, A. Wetscherek, A. Müller, and W. Drube, New J. Phys. **11**, 125007 (2009).
[2]K. Kakushima, K. Okamoto, K. Tachi, J. Song, S. Sato, T. Kawanago, K. Tsutsui, N. Sugii, P. Ahmet, T. Hattori, and H. Iwai, J. Appl. Phys. **104**, 104908 (2008).
[3]X. Li, H. Wang, J. Robinson, H. Sanchez, G. Diankov, and H. Dai, J. Am. Chem. Soc. **131**, 15939–15944 (2009).
[4]I. Saadeddin, H. Hilal, B. Pecquenard, J. Marcus, A. Mansouri, C. Labrugere, M. Subramanian, and G. Campet, Solid State Sci. **8**, 7–13 (2006).
[5]S. Sanchita and S. Umapathy, Sci. Rep. **4**, 5308 (2014).
[6]A. Goldstein, *Handbook of Nanophase Materials, Materials Engineering* (CRC Press, 1997), p. 337.
[7]A. V. Zenkevich, Y. A. Matveyev, Y. Y. Lebedinskii, R. Mantovan, M. Fanciulli, S. Thiess, and W. Drube, J. Appl. Phys. **111**, 07C506 (2012).
[8]C. Leroux, S. Baudot, M. Charbonnier, A. V. D. Geest, P. Caubet, A. Toffoli, P. Blaise, G. Ghibaudo, F. Martin, and G. Reimbold, Solid-State Electron. **88**, 21–26 (2013).
[9]O. Weber, F. Andrieu, J. Mazurier, M. Casse, X. Garros, C. Leroux, F. Martin, P. Perreau, C. Fenouillet-Béranger, S. Barnola, R. Gassilloud, C. Arvet, O. Thomas, J.-P. Noel, O. Rozeau, M.-A. Jaud, T. Poiroux, D. Lafond, A. Toffoli, F. Allain, C. Tabone, L. Tosti, L. Brevard, P. Lehnen, U. Weber, P. Baumann, O. Boissiere, W. Schwarzenbach, K. Bourdelle, B.-Y. Nguyen, F. Boeuf, T. Skotnicki, and O. Faynot, in *IEEE International Electron Device* Meeting (2010), pp. 341–344.
[10]J. Robertson, Solid-State Electron. **49**, 283–293 (2005).
[11]S. Lee, S.-H. Kim, Y. Kim, A. I. Kingon, D. C. Paine, and K. No, Mater. Lett. **85**, 88–90 (2012).
[12]W. Besling, E. Young, T. Conard, C. Zhao, R. Carter, W. Vandervorst, M. Caymax, S. D. Gendt, M. Heyns, J. Maes, M. Tuominen, and S. Haukka, J. Non-Cryst. Solids **303**, 123–133 (2002).
[13]C. E. Kim and I. Yun, Appl. Surf. Sci. **258**, 3089–3093 (2012).
[14]W. Haynes, *Handbook of Chemistry and Physics*, 93rd ed. (CRC Press, 2012).
[15]G. Dingemans, P. Engelhart, R. Seguin, B. Hoex, M. C. M. Van de Sanden, and W. M. M. Kessels, in *Proceedings of the 34th IEEE* Photovoltaic Specialists Conference (*PVSC*) (2009), pp. 705–708.
[16]M. P. Seah, Surf. Interface Anal. **14**, 488–488 (1989).
[17]L. A. Walsh, G. Hughes, P. K. Hurley, J. Lin, and J. C. Woicik, Appl. Phys. Lett. **101**, 241602 (2012).
[18]P. Swift, Surf. Interface Anal. **4**, 47–51 (1982).
[19]T. L. Barr and S. Seal, J. Vac. Sci. Technol., A **13**, 1239–1246 (1995).
[20]See supplementary material at http://dx.doi.org/10.1063/1.4919448 for C 1s and Si 1s HAXPES figures.
[21]S. Tanuma, C. J. Powell, and D. R. Penn, Surf. Interface Anal. **43**, 689–713 (2011).
[22]R. Katamreddy, R. Inman, G. Jursich, A. Soulet, A. Nicholls, and C. Takoudis, Thin Solid Films **515**, 6931–6937 (2007).
[23]B. E. Deal, M. Sklar, A. S. Grove, and E. H. Snow, J. Electrochem. Soc. **114**, 266–274 (1967).
[24]J. Rafí, M. Zabala, O. Beldarrain, and F. Campabadal, J. Electrochem Soc. **158**, G108–G114 (2011).
[25]G. Dingemans, N. M. Terlinden, M. A. Verheijen, M. C. M. van de Sanden, and W. M. M. Kessels, J. Appl. Phys. **110**, 093715 (2011).
[26]R. L. Opila, G. D. Wilk, M. A. Alam, R. B. van Dover, and B. W. Busch, Appl. Phys. Lett. **81**, 1788–1790 (2002).
[27]L. Kornblum, J. A. Rothschild, Y. Kauffmann, R. Brener, and M. Eizenberg, Phys. Rev. B **84**, 155317 (2011).
[28]T. Tachibana, T. Sameshima, Y. Iwashita, Y. Kiyota, T. Chikyow, H. Yoshida, K. Arafune, S. Satoh, and A. Ogura, Jpn. J. Appl. Phys., Part 1 **50**, 04DP09 (2011).